The Roles of Glu-327 and His-446 in the Bisphosphatase Reaction of Rat Liver 6-Phosphofructo-2-kinase/Fructose-2,6-bisphosphatase Probed by NMR Spectroscopic and Mutational Analyses of the Enzyme in the Transient Phosphohistidine Intermediate Complex†

David A. Okar, David H. Live, Tara L. Kirby, Elizabeth J. Karschnia, Linda B. von Weymarn, Ian M. Armitage, and Alex J. Lange*

Department of Biochemistry, University of Minnesota, School of Medicine, 435 Delaware Street SE, Minneapolis, Minnesota 55455

Received December 7, 1998; Revised Manuscript Received February 8, 1999

ABSTRACT: The bisphosphatase domain derived from the rat liver 6-phosphofructo-2-kinase/fructose-2,6-bisphosphatase was studied by $^{1}H-^{13}C$ HMQC NMR spectroscopy of the histidine C2′ and H2′ nuclei. The bacterially expressed protein was specifically labeled with ^{13}C at the ring C2′ position of the histidines. Each of the seven histidine residues gave rise to a single cross-peak in the HMQC spectra, and these were assigned by use of a series of histidine-to-alanine point mutants. His-304, His-344, and His-469 exhibit ^{13}C and ^{1}H resonances that titrated with pH, while the remaining histidine-associated resonances did not. The ^{13}C and ^{1}H chemical shifts indicate that at neutral pH, His-304 and His-446 are deprotonated, while His-469 is protonated. The pK_a* of His-344 was determined to be 7.04. The ^{13}C chemical shifts suggest that the deprotonated His-258 exists as the N1′ tautomer, while His-392 and His-419 are protonated in the resting, wild-type enzyme. Mutation of the remaining member of the catalytic triad, Glu-327, to alanine in the resting enzyme caused an upfield shift of 1.58 and 1.30 ppm in the ^{1}H and ^{13}C dimensions, respectively, and significant narrowing of the His-258 cross-peak. Mutation of His-446 to alanine produced perturbations of the His-258 cross-peak that were similar to those detected in the E327A mutant. The His-392 resonances were also shifted by the E327A and H446A mutations. These observations strongly suggest that residues His-258, Glu-327, His-392, and His-446 exist within a network of interacting residues that encompasses the catalytic site of the bisphosphatase and includes specific contacts with the C-terminal regulatory region of the enzyme. The specifically ^{13}C-labeled bisphosphatase was monitored during turnover by HMQC spectra acquired from the transient N3′ phosphohistidine intermediate complex in the wild-type enzyme, the E327A mutant, and the H446A mutant. These complexes were formed during reaction with the physiological substrate fructose-2,6-bisphosphate. Upon formation of the phosphohistidine at His-258, the ^{13}C and ^{1}H resonances of this residue were shifted downfield by 1.7 and 0.31 ppm, respectively, in the wild-type enzyme. The upfield shifts of the His-258 resonances in the E327A and H446A mutant resting enzymes were reversed when the phosphohistidine was formed, generating spectra very similar to that of the wild-type enzyme in the intermediate complex. In contrast, the binding of fructose-6-phosphate, the reaction product, to the resting enzyme did not promote significant changes in the histidine-associated resonances in either the wild-type or the mutant enzymes. The interpretation of these data within the context of the X-ray crystal structures of the enzyme is used to define the role of Glu-327 in the catalytic mechanism of the bisphosphatase and to identify His-446 as a putative link in the chain of molecular events that results in activation of the bisphosphatase site by cAMP-dependent phosphorylation of the hepatic bifunctional enzyme.

The bifunctional enzyme 6-phosphofructo-2-kinase/fructose-2,6-bisphosphatase (6-PF-2-K/F-2,6-P_2ase)[1] plays a major role in the control of hepatic gluconeogenic/glycolytic fluxes because it is the sole enzyme responsible for both the synthesis and degradation of fructose-2,6-bisphosphate and thereby modulates the intracellular concentration of this signal metabolite (*1, 2*). Fructose-2,6-bisphosphate is an allosteric activator of 6-phosphofructo-1-kinase and an allosteric inhibitor of fructose-1,6-bisphosphatase; therefore, its cytosolic concentration is a primary determinant of carbohydrate flux in liver (*3*). The kinase and bisphosphatase reactions take place at two distinct sites within the 55 kDa rat liver bifunctional enzyme, with the kinase domain in the N-terminal region and the bisphosphatase domain in the C-terminal region (*4, 5*). The concentration of F-2,6-P_2 is determined by the relative activities of the domains. The kinase-to-bisphosphatase activity ratio (K/BP) is dependent upon the phosphorylation state of Ser-32 (*6*). The modulation of the bisphosphatase reaction by phosphorylation at Ser-32 is mediated by interaction of the N- and C-terminal regions

† This work was supported by NIH Grant R01-DK38354-11 to A.J.L.

* To whom correspondence should be addressed. E-mail: lange@brain.biochem.umn.edu.

10.1021/bi9828728 CCC: $18.00
Published on Web 03/18/1999

of the bifunctional enzyme (*7*−*10*). The cAMP-dependent phosphorylation of Ser-32 is mediated by glucagon, while glucose promotes dephosphorylation via a xyulose-5-phosphate-dependent protein phosphatase (*6*, *11*). Phosphorylated bifunctional enzyme has a low K/BP and functions to lower F-2,6-P_2 levels, while dephosphorylated enzyme has a high K/BP and serves to increase F-2,6-P_2 levels. Therefore, the opposing actions of insulin and glucagon on hepatic carbohydrate flux can be understood, at least in part, by their modulation of the K/BP of the bifunctional enzyme.

The separately expressed rat liver bisphosphatase domains are devoid of kinase activity, yet possess steady-state bisphosphatase activity very similar to the dephosphorylated bifunctional enzyme (*12*, *13*). The bisphosphatase hydrolyzes F-2,6-P_2 to F-6-P and P_i via a covalent N3′ phosphohistidine intermediate at His-258 (*14*−*16*). The active site contains a catalytic triad consisting of His-258, Glu-327, and His-392 (*17*), and the recent X-ray crystal structure of the ND249CT30 bisphosphatase domain detected a water molecule bound to the Glu-327 residue (*18*). The X-ray crystal structures of the resting enzyme (ND249CT30) and the phosphohistidine intermediate complex have also been determined (*18*, *19*). The X-ray crystal structure of a rat testis bifunctional enzyme confirmed that the separate bisphosphatase domain has the native structure (*20*). Based on the X-ray structures and steady-state kinetic data, Lee et al. proposed a mechanism for F-2,6-P_2 hydrolysis that requires a deprotonated His-258 to attack the 2-phospho group of F-2,6-P_2 and form the N3′ phosphohistidine intermediate. A protonated His-392 is required to donate a proton to the F-6-P leaving group and complete the formation of the transient intermediate. The reaction is completed when the water bound to a deprotonated Glu-327 attacks the phosphohistidine and hydrolyzes it by way of a pentavalent, trigonal bipyramidal intermediate and releases the P_i (*18*, *19*).

Previous NMR and crystallographic studies have indicated that the E−P:F-6-P complex is predominant during turnover and can be visualized by these techniques (*16*, *18*, *19*). Herein, we have used 2D NMR spectroscopy of ND249 samples that had been specifically labeled with ^{13}C at the ring C2′ of the histidines to probe the chemical environment of these residues and, thereby, map the interactions within the catalytic site and assess the protonation and tautomeric states of the histidines (*21*−*24*). The ND249 bisphosphatase domain contains seven histidine residues, and the environment of each was addressed by use of an alanine point-mutant engineered for each histidine in the bisphosphatase domain. Of the seven histidines, two are located at the active site (His-258 and His-392), two are in the regulatory C-terminal region of the enzyme (His-446 and His-469), and the remaining residues (His-304, His-344, and His-419) are scattered throughout the bisphosphatase domain. All but His-304 are conserved in the rat testis isoform, where it is replaced by glutamine (*25*). The pH* dependence of the $^1H-^{13}C$ HMQC spectrum for the wild-type ND249 was used to address the pK_a* values of the histidines. The role of Glu-327 in catalysis was probed by HMQC spectroscopy of the [^{13}C]histidine-labeled E327A mutant. Further, these studies included HMQC analyses of the transient phosphohistidine intermediate complex in the wild-type as well as the E327A and H446A mutants.

EXPERIMENTAL PROCEDURES

Mutagenesis. All pET3a plasmids encoding the nine mutants of the ND249 bisphosphatase domain used in this study were constructed from expression plasmids for the bifunctional and bisphosphatase domain constructs from previous studies in our laboratory (*13*, *16*, *17*, *26*). Source plasmid DNA was prepared from BMH 71/18 *E. coli* cultures by anion exchange (Qiagen, Chatsworth, CA). The expression plasmid for the ND249.E327A mutant was prepared by digestion of the pET3a vector encoding the bifunctional enzyme mutant with Nco I and Hind III and ligation of the resulting 906 base pair fragment into the Nco I and Hind III digested ND249.WT pET3a vector. All other single point mutants were constructed from the pET3a vector encoding ND249.WT and oligonucleotide primers designed to introduce the desired mutations by either the PCR-based Megaprimer method (*27*) or the QuickChange site-directed mutagenesis kit (Stratagene, La Jolla, CA). All candidate plasmids were transformed into BMH 71/18 cells and then purified for automated DNA sequencing (ABI 373, Perkin-Elmer, Foster City, CA) to confirm the presence of the mutations. Finally, the expression plasmids were transformed into BL21(DE3) his$^-$ *E. coli* for production of specifically labeled protein (*26*).

Protein Expression, Purification, and Determination. The wild-type and mutant bisphosphatase domains were specifically labeled with ^{13}C at the ring C2′ of the histidine residues by expression from the BL21(DE3) his$^-$ strain harboring a pET3a expression vector as described previously (*26*). The sole histidine source during the induction phase was 99.9%-enriched C2′[^{13}C]histidine (Cambridge Isotope Laboratory, Andover, MA). The proteins were purified by anion exchange and gel filtration chromatography by the methods previously reported (*16*, *26*). All samples were >95% pure based on SDS/PAGE analysis. Protein concentration was determined by the BCA assay (Pierce, Rockford, IL).

NMR Sample Preparation. The NMR samples were prepared from purified protein that had been dialyzed against 100 mM sodium phosphate, pH 8.0. The samples were concentrated by ultrafiltration through YM10 membranes and Centricon-10 microconcentrators (Amicon, Beverly, MA). After concentration, the samples were exchanged into 100 mM sodium phosphate, 0.02% azide, and 99.9% D_2O at the appropriate pH* by dilution in the D_2O buffer and reconcentration. The sample was then dialyzed against the same buffer overnight with frequent changes. The concentration of the resulting samples was between 0.6 and 2.0 mM. Because addition of concentrated DCl or NaOD to the samples caused significant precipitation of the protein, the

[1] Abbreviations: 6-PF-2-K/F-2,6-P_2ase, 6-phosphofructo-2-kinase/fructose-2,6-bisphosphatase; ND249, bisphosphatase domain derived by N-terminal deletion of 249 amino acids from the rat liver bifunctional enzyme; ND249CT30, bisphosphatase domain derived from ND249 by C-terminal truncation of 30 amino acids; F-6-P, fructose-6-phosphate, F-2,6-P_2, fructose-2,6-bisphosphate; K/BP, kinase-to-bisphosphatase activity ratio; P_i, inorganic phosphate ion; HMQC, heteronuclear multiple quantum correlation; pH*, pH in D_2O; pK_a*, acid dissociation constant in D_2O; NIDDM, non-insulin-dependent diabetes mellitus; HGO, hepatic glucose output. The numbering of all amino acid residues refers to the rat liver 6-PF-2-K/F-2,6-P_2ase. The imidazole ring of histidine is numbered according to the common biochemical scheme: N1′ = $N^{\delta 1}$, C2′ = $C^{\epsilon 1}$, N3′ = $N^{\epsilon 2}$, C4′ = $C^{\delta 2}$, and C5′ = C^{γ}.

pH titration was accomplished by preparation of a series of NMR samples over the pH* range 5.4−9.2. Fructose-2,6-bisphosphate and fructose-6-phosphate were introduced at a 10× molar excess relative to enzyme by microliter additions of concentrated stock solutions prepared in the NMR buffer. The additions were made in an Eppendorf tube, and the sample was quickly transferred to the NMR tube and placed in the magnet. All comparisons of the data acquired after addition of F-2,6-P_2 or F-6-P were made between sample aliquots from a single pool of purified and prepared bisphosphatase. Measurements of the pH throughout sample preparation and after spectral acquisition agreed within 0.12 unit.

NMR Spectroscopy. Phase-sensitive $^1H-^{13}C$ HMQC data were collected on a Varian INOVA 600 MHz spectrometer with a 5 mm HCN triple resonance probe at 15 °C (*28*). Typical conditions employed a proton spectral width of 10 000 Hz and an acquisition time of 0.17 and 32 scans/increment for a total acquisition time of 1.5 h. The carbon spectral width was 2000 Hz with 70 increments in the ^{13}C dimension. Spectra were decoupled in both dimensions. Chemical shifts for ^{13}C were referenced from the ^1H shift scale, based on the position of the HOD signal, using the method of Wishart et al. (*29*). Data were processed with the Vnmr software (Varian, Palo Alto, CA).

RESULTS

Resonance Assignments. The 2D HMQC experiment allowed resolution of all seven cross-peaks from the labeled histidines. Each of the histidine C2′ and H2′ resonances in the ND249 bisphosphatase domain were assigned by HMQC spectroscopy using a series of His→Ala point mutants. For example, the series of HMQC spectra obtained for ND249.WT, ND249.H258A, and ND249.H258A.H392A at pH* 7.0 are shown in Figure 1A−C. The resonances were assigned based on the loss of a single resonance upon each His→Ala mutation. In some cases the mutation caused chemical shift changes in the resonances of other histidine residues; therefore, the saturation mutagenesis of the histidines ensured the accuracy of the assignments. The chemical shifts of the histidine resonances in the wild-type resting enzyme are summarized in Table 1.

Mutational Analyses. The chemical shift changes resulting from each mutation are depicted by the $\Delta\delta$ plots in Figure 2A−F. These show the changes in ^{13}C and ^1H chemical shifts in each mutant relative to the ND249.WT in 100 mM sodium phosphate, pH* 7.0. The H304A, H344A, H419A, and H469A mutations did not significantly perturb the resonances of the other histidines, while the H258A and H446A mutations had significant and specific effects upon the resonances of the catalytic histidines. These observations confirm that the histidine mutations did not compromise the global structure of the enzyme; rather, the effects were localized to the microenvironment of each histidine.

The HMQC spectrum of the ND249.E327A mutant is shown in Figure 3A. The accompanying $\Delta\delta$ plot (Figure 3B) demonstrates that replacement of Glu-327 with alanine strongly perturbed the His-258 chemical shifts and, to a much lesser extent, those of His-392. All other histidine resonances were virtually unperturbed by the E327A mutation. Because the cross-peaks for both catalytic histidine residues were shifted in the ND249.E327A mutant, we used a double mutant, ND249.H258A.E327A, to unambiguously assign the catalytic histidine resonances in that mutant (data not shown). The most striking feature of the E327A mutant is the significant upfield shift in the phosphoacceptor, His-258, resonance in both the ^1H and ^{13}C dimensions.

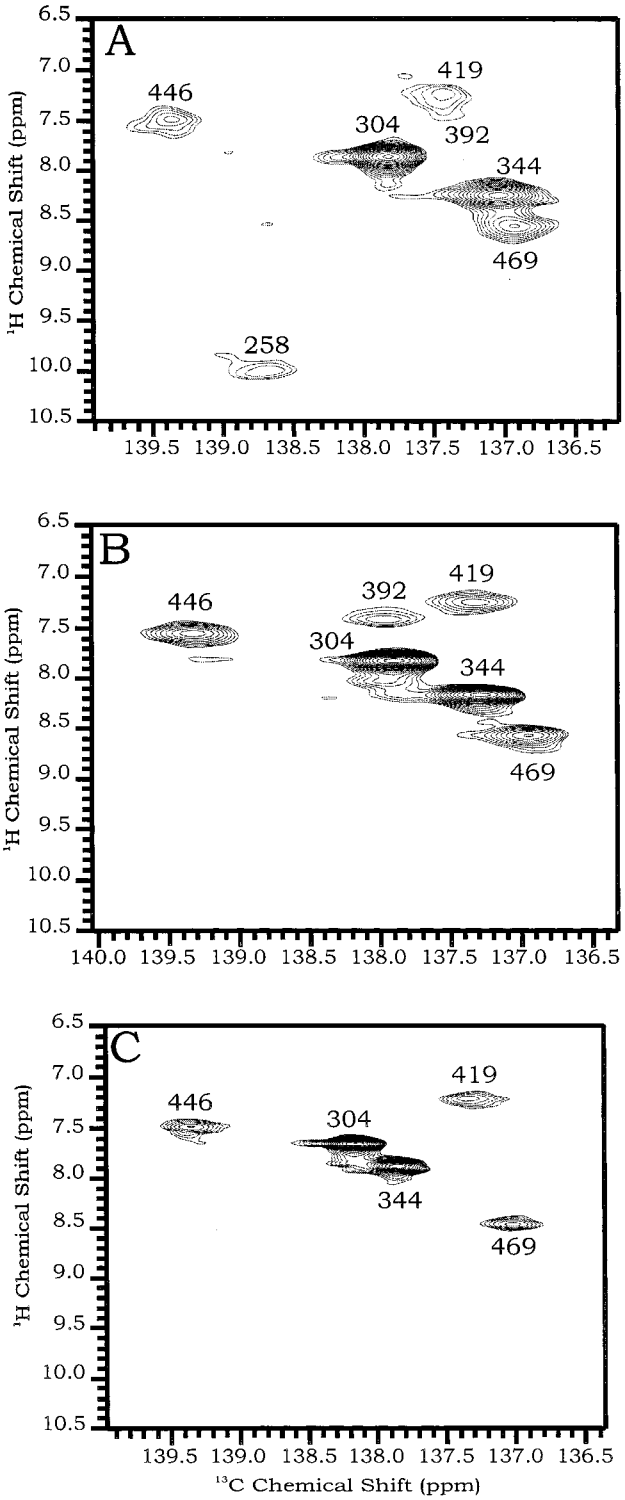

FIGURE 1: HMQC spectra used to assign the catalytic histidines. The data acquisition and sample conditions were as stated under Experimental Procedures. The data were acquired for the following enzymes: spectrum A; wild-type bisphosphatase (ND249.WT); B, the single point mutant ND249.H258A; and C, the double mutant ND249.H258A.H392A.

Table 1: Histidine Ring C2′ Chemical Shifts in the Wild-Type Fructose-2,6-bisphosphatase Domain at 100 mM Sodium Phosphate, pH* 7.0 and 15 °C[a]

histidine	^{13}C shift (ppm)	^{1}H shift (ppm)
258	138.4	9.89
304	138.0	7.75
344	137.3	8.00
392	137.3	7.14
419	137.3	7.25
446	136.9	8.50
469	139.2	7.47
protonated	≤136.5	≥8.50
deprotonated	≥138.0	≤7.5

[a] The chemical shifts given for protonated and deprotonated histidine residues at neutral pH were derived from those reported in the literature (*21*−*23, 31, 33, 35*−*39*).

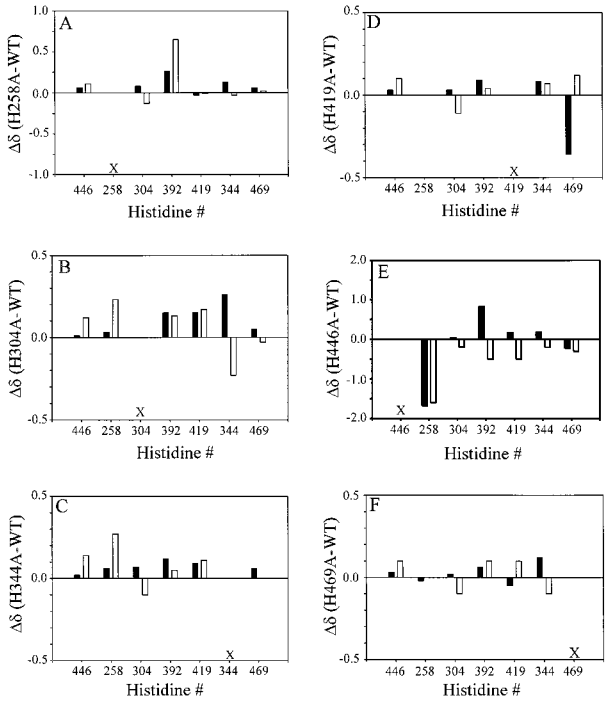

FIGURE 2: Δ*δ* plots derived from HMQC spectra of the entire series of His→Ala point mutants. The Δ*δ* values were determined by subtracting the chemical shifts associated with each histidine residue in each mutant from those of the same residue in the wild-type enzyme. Plot A, H258A; B, H304A; C, H344A; D, H419A; E, H446A; and F, H469A. The ^{13}C shifts are in open bars and ^{1}H shifts in filled bars. Note that the scales of the plots are different because the chemical shift changes produced by the H258A and H446A mutations are much larger than those detected in the other mutants.

Titration of Histidine Residues with pH. The pH* dependencies of the assigned C2′ ^{13}C and ^{1}H resonances for each histidine in ND249.WT were determined by HMQC spectroscopy of a series of samples of specifically labeled bisphosphatase domain over the range pH* 5.4−9.2. As shown in Figure 4A,B, His-304, His-344, and His-469 have pH*-dependent ^{1}H and ^{13}C chemical shifts corresponding to freely titrating residues. The shifts of both the ^{13}C and ^{1}H resonances with the change in pH* paralleled those reported for these same nuclei in other proteins (*21, 22, 30*−*34*). The remaining histidine-associated resonances did not shift with pH (data not shown). The pK_a* values determined from these titration data and those estimated for the nontitrating residues are given in Table 2.

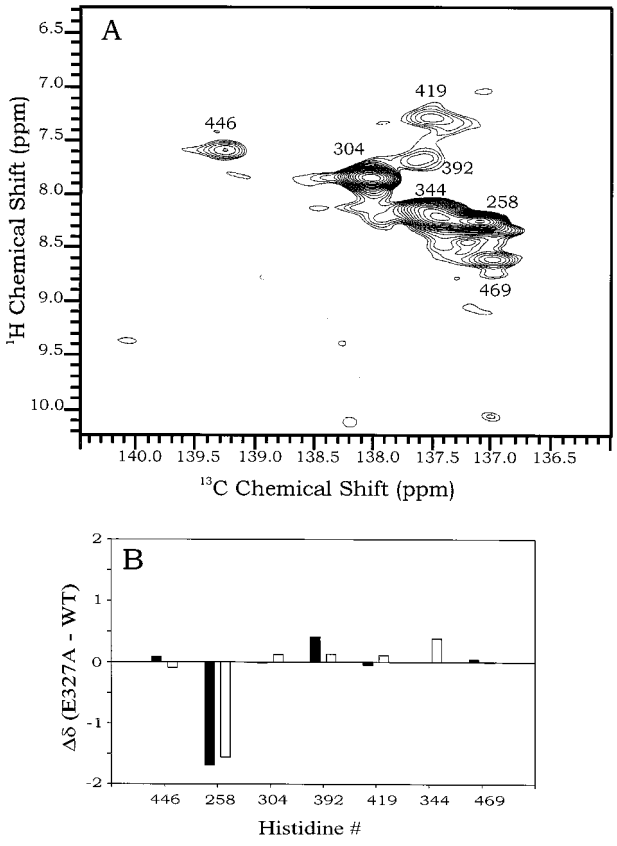

FIGURE 3: HMQC data of the ND249.E327A mutant. The data were acquired under the conditions indicated under Experimental Procedures. The HMQC spectrum is presented in panel A, and the corresponding Δ*δ* plot is given in panel B. The Δ*δ* values were determined as (mutant − wild-type) chemical shifts. The ^{13}C shifts are in open bars and ^{1}H shifts in filled bars.

The Bisphosphatase Domain during Turnover. When excess F-2,6-P_2 is added to the wild-type bisphosphatase domain, the transient, phosphohistidine-containing, intermediate E−P:F-6-P forms within 80 ms and remains at steady-state for at least 6−8 h (*15, 16*). Therefore, during the time required for acquisition of the current NMR data, the enzyme exists primarily in the E−P:F-6-P complex at the steady-state level. The HMQC spectrum of the wild-type bisphosphatase domain in the presence of a 10× molar excess of F-2,6-P_2 is shown in Figure 5A. These data clearly indicate that the His-258 resonances are shifted downfield in both dimensions and that the His-392 ^{13}C resonance is shifted upfield by the formation of the phosphohistidine intermediate. These spectral changes are not related simply to the binding of F-6-P, because concurrent HMQC analyses of the enzyme in the presence of a 10× molar excess of F-6-P did not perturb any of the histidine resonances.

The HMQC spectrum of ND249.E327A in the presence of excess F-2,6-P_2 is very similar to that of the wild-type enzyme in the E−P:F-6-P complex, as shown in Figure 6A. The Δ*δ* plot in Figure 6B depicts the chemical shift changes that result from formation of the phosphohistidine intermediate in the E327A mutant. Upon formation of the transient intermediate in the E327A mutant, the resonances assigned to the His-258 phosphoacceptor show large changes in the chemical shifts. These completely reverse the upfield shifts noted in the mutant resting enzyme and, in addition, demonstrate the shifts seen for the intermediate complex with

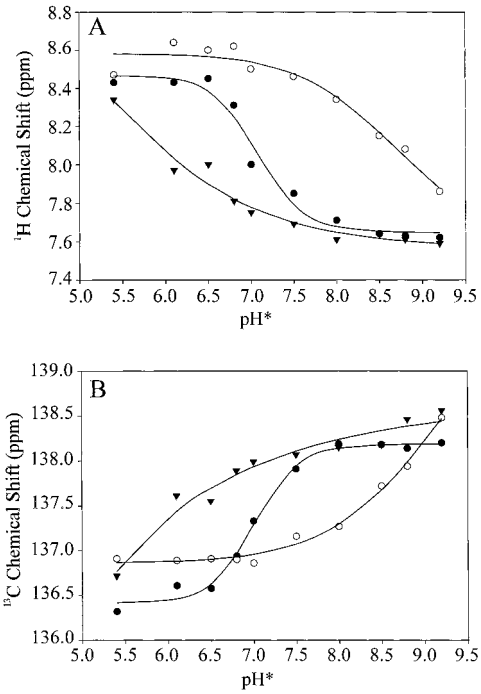

FIGURE 4: pH* titration of the C2′ histidine-associated ^{1}H−^{13}C HMQC cross-peaks in 100 mM sodium phosphate at 15 °C. His-304 (▼), His-344 (●), and His-469 (○) titrate in both the proton (panel A) and the carbon (panel B) dimensions. The remaining C2′ histidine cross-peaks do not titrate.

Table 2: Characteristics of the Histidine Residues in the Bisphosphatase Domain

histidine	protonation state at pH* 7.0	pK_a*	tautomeric state
258	neutral	<7.0[a]	N1′
304	neutral	<6.0[b]	N3′
344	neutral	7.04[b]	N3′
392	cationic	>7.0[a]	–
419	cationic	>7.0[a]	–
446	neutral	<7.0[a]	N3′
469	cationic	>8.5[b]	–

[a] Predicted from the ^{13}C chemical shifts of the C2′ resonances at pH* 7.0. [b] Determined from the pH titration of the ^{13}C and ^{1}H chemical shifts of the C2′ resonances.

the wild-type enzyme (see Figure 5B). The effect of the E327A mutation on the E−P:F-6-P complex is demonstrated in the Δδ plots in Figure 7A, which compare histidine-associated resonances in the wild-type and E327A mutant for the phosphohistidine intermediate complex. An HMQC spectrum was also acquired for the H446A mutant in the transient phosphohistidine intermediate, and the Δδ plot for comparison of this complex to that in the wild-type enzyme is shown in Figure 7B. In contrast to those seen in the resting enzyme, the effects of the E327A and H446A mutations on the HMQC spectra of the phosphohistidine intermediate are slight. The presence of the covalent phosphohistidine intermediate in these mutants was confirmed by parallel studies with 2[^{32}P]F-2,6-P_2 (data not shown) and a previous report (*17*). The ^{13}C and ^{1}H chemical shifts for the C2′ and H2′ nuclei in the phosphohistidine intermediate for the wild-type, E327A, and H446A are summarized in Table 3.

DISCUSSION

The seven histidine residues within the wild-type bisphosphatase domain are located in a variety of chemical

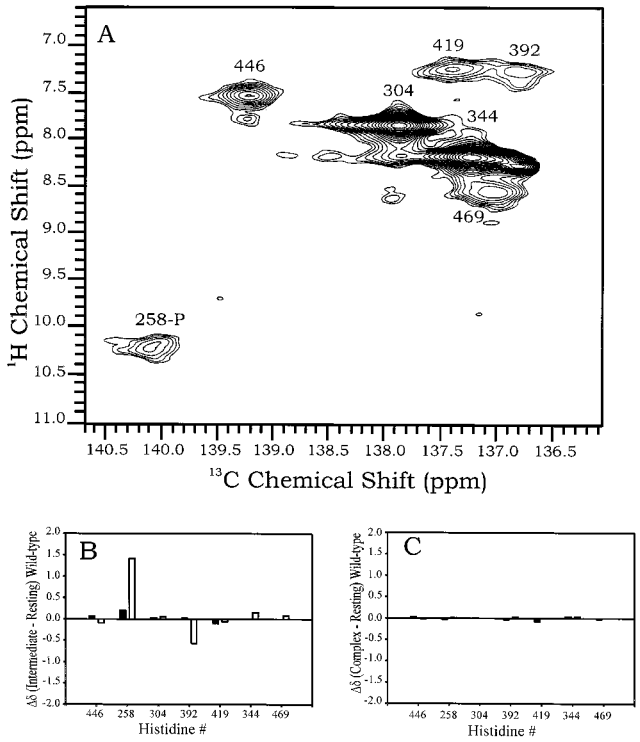

FIGURE 5: HMQC data of the ND249.WT bisphosphatase domain in complexes with F-6-P and in the phosphohistidine intermediate. The HMQC spectrum acquired under the conditions indicated under Experimental Procedures is presented in panel A. The Δδ plots were calculated by subtracting the chemical shifts of the resting enzyme (Table 1) from those determined from the spectra of ND249.WT in the presence of excess F-2,6-P_2 (E−P:F-6-P) (panel B) and in the presence of excess F-6-P (panel C). The ^{13}C shifts are in open bars and ^{1}H shifts in filled bars.

environments as evidenced by the range of chemical shifts observed in the HMQC profile. On the basis of the pH* titration data, the histidines in the bisphosphatase fall into two classes. His-304, His-344, and His-469 titrated with pH*, while His-258, His-392, His-419, and His-446 did not. These results correlate with the X-ray structures which show that the titratable histidine residues are located at or near the surface, while the nontitratable His-258, His-392, and His-419 are buried within the macromolecule (*18*−*20*). Only His-446 is anomalous in this analysis, since it is located at the surface and does not titrate.

The C2′ and H2′ chemical shifts characteristic of protonated and deprotonated histidine residues culled from the literature are listed in Table 1 (*21*−*23, 31, 33, 35*−*39*). The deprotonated histidine is assumed to exist in the more stable N3′ tautomer, which is likely for solvent-accessible residues (*31*). According to the published reports, the ^{13}C chemical shift of the C2′ is unaffected by the tautomeric state of the histidine, while the ^{1}H chemical shift of the H2′ resonance is sensitive to tautomerization (*31, 34*). Therefore, the ^{13}C chemical shift may be a better predictor of the protonation state than the ^{1}H chemical shift at the C2′ position. However, numerous reports indicate that the ^{13}C and ^{1}H chemical shifts of these nuclei may be significantly perturbed by strong hydrogen bonding and other microscopic interactions of the histidines (*21, 22, 31, 33, 36, 39*−*41*). Bearing these caveats in mind, we used the C2′ ^{13}C chemical shifts to predict the protonation states of the nontitratable histidines in the bisphosphatase domain. These are listed in Table 2. To more

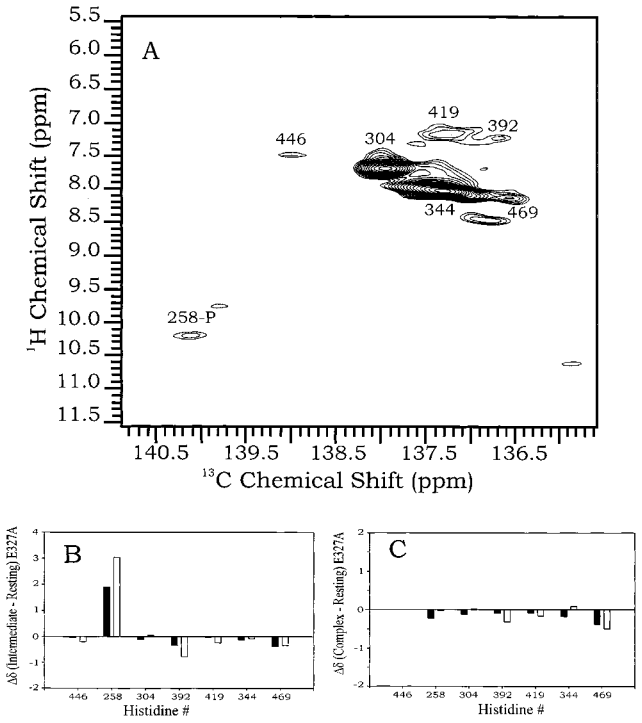

FIGURE 6: HMQC data of the ND249.E327A point mutant in complexes with F-6-P and in the phosphohistidine intermediate. The HMQC spectrum acquired under the conditions indicated under Experimental Procedures is presented in panel A. The $\Delta\delta$ plots were calculated by subtracting the chemical shifts of the resting enzyme from those determined from the spectra of ND249.WT in the presence of excess F-2,6-P_2 (E−P:F-6-P) (panel B) and in the presence of excess F-6-P (panel C). The ^{13}C shifts are in open bars and ^{1}H shifts in filled bars.

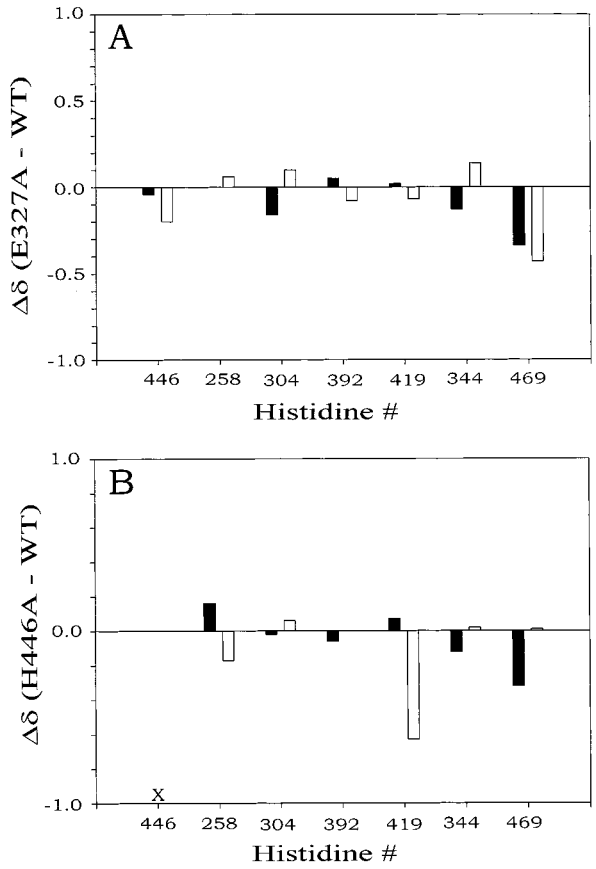

FIGURE 7: Structural changes promoted by turnover of the bisphosphatase domain. These $\Delta\delta$ plots were derived from HMQC spectra acquired under the conditions described under Experimental Procedures. The plots were calculated by subtracting chemical shifts determined for the wild-type enzyme from those of the E327A (panel A) and the H446A (panel B) mutants in the phosphohistidine intermediate. The ^{13}C shifts are in open bars and ^{1}H shifts in filled bars.

fully define the protonation states of the histidine residues, especially those at the catalytic site, our ongoing studies will employ site-specific ^{15}N labeling of the imidazole nitrogens.

The phospho-His-258 intermediate in the bisphosphatase reaction has been shown by both ^{1}H−^{31}P HMQC spectroscopy and X-ray crystallography to be the N3′ phosphoramidate adduct (*16*, *19*). This requires that deprotonated His-258 be stabilized as the energetically disfavored N1′ tautomer, thereby directing the phosphorylation to the N3′ position. In this respect, His-258 is similar to His-57 in chymotrypsinogen in which the N1′ tautomer is stabilized by hydrogen bonding to Asp-102 (*24*, *41*). The chemical shift observed for the ^{1}H resonance of His-258 in the bisphosphatase is similar to that of ≈9.2 ppm reported for His-57 in chymotrypsinogen, consistent with the existence of His-258 in the N1′ tautomeric form.

The E327A and H446A mutant bisphosphatases were notable for their specific and significant perturbation of the resonances assigned to the catalytic histidines. This was expected for the E327A mutant based on the location of Glu-327 in the catalytic triad at the heart of the bisphosphatase active site. However, the observation that mutation of His-446 caused significant perturbation of the cross-peaks assigned to His-258 and His-392 was unexpected. Mutation of either Glu-327 or His-446 lead to an upfield shift in both dimensions for the His-258 resonance. The His-258 cross-peak is also significantly narrower in the HMQC spectra of the mutants. Although similar, the spectral perturbations of the His-258 cross-peak produced in the two mutants are not identical ($\Delta\delta$ ^{13}C = −1.6; ^{1}H = −1.68 for H446A and ^{13}C = −1.3; ^{1}H = −1.58 for E327A). Furthermore, comparison of the spectral perturbations at the other histidines (Figures 2E and 3B) indicates that while the H446A mutation perturbs the His-392, His-419, and His-469 cross-peaks, the effect of the E327A mutation is restricted to the catalytic histidines. These spectral differences reflect the different roles of these residues in the bisphosphatase reaction. A number of mechanisms may account for the upfield shift of the His-258 resonances in these mutants; however, the simplest explanation is that the mutation of these residues promotes an increase in the pK_a of His-258; i.e., the phospho acceptor is deprotonated in the wild-type and protonated in the mutants (based on ^{13}C chemical shifts). If this is the case, then His-

Table 3: Histidine Ring C2′ Chemical Shifts in the Transient Phosphohistidine Intermediate of the Fructose-2,6-bisphosphatase Domain at 100 mM Sodium Phosphate, pH* 7.0 and 15 °C, for the Wild-Type, E327A, and H446A Enzymes

	wild-type		E327A		H446A	
histidine	^{13}C	^{1}H	^{13}C	^{1}H	^{13}C	^{1}H
258	140.1	10.20	140.1	10.20	139.9	10.30
304	137.8	7.86	137.9	7.70	137.9	7.82
344	137.2	8.19	137.3	8.06	137.2	8.10
392	136.8	7.26	136.7	7.31	136.8	7.15
419	137.3	7.23	137.3	7.25	136.7	7.32
446	139.2	7.54	139.0	7.50	−	−
469	137.0	8.52	136.6	8.20	137.0	8.20

258 should be titratable in the E327A and H446A mutants. Unfortunately, these mutants had a severely reduced pH* range over which HMQC spectra could be acquired, due to precipitation of the protein upon titration; therefore, the histidine resonances in the mutants could not be titrated. Both mutants are still active bisphosphatases. This observation and the site-specific nature of the chemical shift perturbations induced by the mutations imply that they do not cause gross structural changes; rather, they specifically alter the chemical environment of the catalytic site. These data suggest that the E327A and the H446A mutations result in a disruption of the intramolecular forces that stabilize His-258 in the deprotonated state within the wild-type enzyme. The determination of the exact nature of these intramolecular forces and the status of His-258 are the focus of our continuing NMR studies.

The kinetic consequences of the E327A and H446A mutations are quite different. The role of Glu-327 has been well-studied by steady-state kinetic analyses and point-mutagenesis in the rat liver bifunctional enzyme. The rate of phosphohistidine intermediate formation was reduced 1000-fold in the E327A mutant, and the V_{max} was just 4% of the wild-type enzyme. The K_m for F-2,6-P_2 and the K_i for F-6-P were unchanged (*17*). These results have been corroborated by preliminary kinetic analyses of the ND249.E327A mutant based on formation of ^{32}P-labeled enzyme after addition of 2[^{32}P]F-2,6-P_2. The rate of phosphohistidine formation as well as the steady-state level of the intermediate are significantly reduced in the ND249.E327A mutant (data not shown). In contrast, the same kinetic analyses of the ND249.H446A mutant suggest that neither the rate of phosphohistidine formation nor the steady-state level of the intermediate is affected; rather, the V_{max} may be increased (data not shown). The putative protonation of His-258 in these mutants is consistent with these kinetic effects. In the case of ND249.H446A, the proposed change in the protonation state of His-258 does not affect the rate-limiting step of the reaction, which has been shown to be dissociation of the F-6-P from the transient intermediate complex (*15, 16, 42*). Increased activity in a mutant bisphosphatase domain may not be paradoxical, given that the ND249.WT functions such as the bisphosphatase in the dephosphorylated (i.e., inhibited) bifunctional enzyme. The proposed change in the protonation state of His-258 in the ND249.E327A mutant may account for the slower rate of phosphohistidine formation; however, in the context of the ND249.H446A results, this alteration of His-258 cannot fully explain the kinetic consequences of the E327A mutation. This is in accord with the data presented here and published reports which demonstrate a direct role for Glu-327 in the formation of the phosphohistidine intermediate.

The mechanism by which phosphorylation of Ser-32 is communicated to the bisphosphatase site is not known, but it is mediated by the termini of the bifunctional enzyme (*7, 8, 43*). The crystal structure of the rat testis bifunctional enzyme dimer showed a head-to-head quaternary structure with numerous intersubunit interactions between the kinase domains, but none between the bisphosphatase domains (*20*). This implies that any inhibition of the bisphosphatase site by the C-terminal region occurs by an intramolecular mechanism. The same bifunctional enzyme structure also shows that a hydrogen bond network ties the His-446 to the

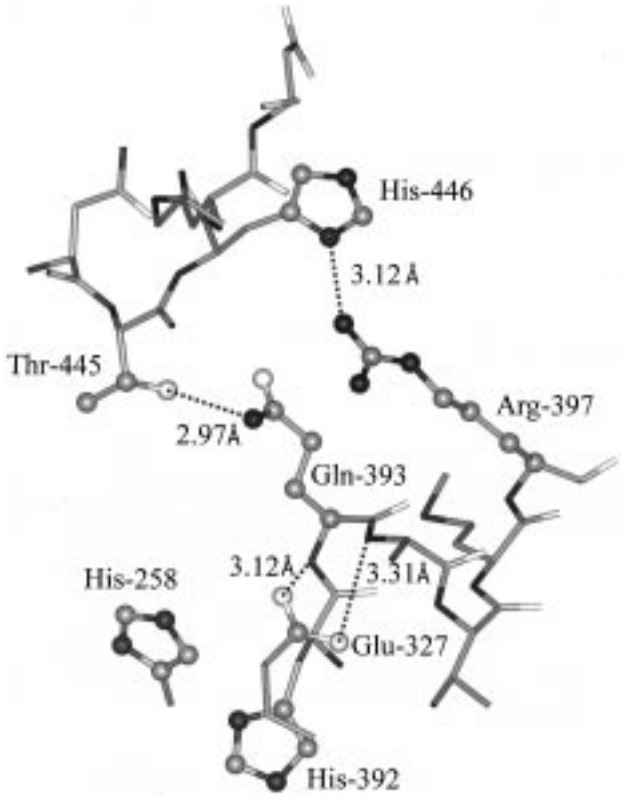

FIGURE 8: View of the rat testis bisphosphatase domain showing the hydrogen bond interactions between the C-terminal residues (His-446 and Thr-445) and residues near the catalytic site. The rat testis structure was determined by Haseman et al., and the coordinates were obtained from the Protein Data Base maintained by Brookhaven National Laboratory (*20*). The residue numbering was converted to that of the rat liver enzyme by adding 2 to each residue number in the rat testis protein. That is, His-444(testis) ≡ His-446(liver) and His-390(testis) ≡ His-392(liver).

catalytic site. As depicted in Figure 8, His-446 forms a hydrogen bond to Arg-397 and Thr-445 to Gln-393. These hydrogen bonds link His-446 and Thr-445 to a region adjacent to the catalytic His-392. Furthermore, the stretch from His-392 to Arg-397 is also hydrogen bonded to Glu-327 via the backbone αNH groups of Ala-394 and Val-395 (*20*). The X-ray structures of the phosphohistidine intermediate complex (E−P:F-6-P) and the E:F-6-P complex obtained with the truncated rat liver bisphosphatase domain, ND249CT30, show that Gln-393 is hydrogen bonded to the phosphate of the phosphohistidine and that Arg-397 is hydrogen bonded to the C6 phosphate of F-6-P, respectively (*19, 44*).

The NMR pH* titration study has identified His-446 as a unique surface residue because it does not titrate. In the context of the X-ray structural data, this result indicates that the hydrogen bond between His-446 and Arg-397 stabilizes the histidine in the deprotonated neutral form. The observation of specific perturbation of the chemical environment at the catalytic site by mutation of His-446 suggests that this hydrogen bond linkage is important in maintaining the stability of the active site. These results are intriguing because phosphorylation of Ser-32 leads to an increased bisphosphatase activity and the mutation of His-446, which is located in the C-terminal region, appears to have the same effect. Unfortunately, the X-ray structures of the truncated bisphosphatase domain do not contain the C-terminal residues that include His-446, and those of the rat testis bifunctional

enzyme were only determined for the resting enzyme. These NMR data bridge this gap and define a putative role for His-446 (and Thr-445) in the activation of the bisphosphatase reaction by cAMP-dependent phosphorylation of Ser-32.

It has been shown by a variety of methods that the dissociation of F-6-P from the phosphohistidine intermediate complex is the rate-limiting step of the reaction, and it is the extreme stability of this complex that is responsible for the long lifetime of the transient intermediate (*15*, *16*, *42*). The crystal structures indicate that Arg-397 can hydrogen bond to both His-446 and the C6 phosphate of F-6-P, and our NMR data show that when the interaction between His-446 and Arg-397 is broken by mutation the resulting structural alterations specifically perturb the chemical shifts of the catalytic histidines. Taken together, these data suggest that the C-terminal domain may inhibit the bisphosphatase by stabilizing the interaction of F-6-P with the phosphohistidine intermediate and may activate the bisphosphatase by disrupting the Arg-397/F-6-P interaction upon cAMP-dependent phosphorylation of Ser-32. This might activate the bisphosphatase by allowing the F-6-P to dissociate from the phosphohistidine intermediate more readily.

In contrast to the resting enzyme, neither the E327A nor the H446A mutation significantly perturbed the His-258 or His-392 resonances in the spectra acquired when the bisphosphatase was in the transient intermediate complex, E−P:F-6-P (see Figure 7). According to the bisphosphatase mechanism proposed by Lee et al., the His-258 nucleophile is stabilized in the deprotonated form and attacks the C2 phosphate group of the substrate to form the transient 3N′ phosphohistidine intermediate, and protonated His-392 donates a proton to the F-6-P leaving group to complete formation of the intermediate. Subsequently, Glu-327 activates an associated water molecule to promote hydrolysis of the phosphohistidine intermediate (*18*, *19*). The NMR results strongly support this mechanism for the formation of the phosphohistidine intermediate. Further, we provide evidence that the deprotonated His-258 exists as the N1′ tautomer, increasing the nucleophilic potential of the N3′ position toward the C2 phosphate of the substrate. It is not known how this thermodynamically disfavored N1′ tautomer is stabilized within the catalytic site, but the kinetic results and these NMR data suggest that Glu-327 plays a direct role in phosphohistidine formation. However, because the HMQC spectra show that the perturbations caused by the E327A mutation have greater amplitude in the resting state of the enzyme than in the transient intermediate, a direct role for Glu-327 in the hydrolysis of the phosphohistidine is not likely. These NMR data further support the view that dissociation of F-6-P from the E−P:F-6-P complex is rate-limiting. This implies that when F-6-P is bound to the E−P intermediate, attack of water at the phosphoramidate is precluded. Upon dissociation of F-6-P, the phosphohistidine is quickly hydrolyzed by water to regenerate the resting enzyme and produce P_i.

The biophysical studies of this enzyme have enabled us to develop a detailed description of the bisphosphatase active site and provide impetus to consider inhibition of the bisphosphatase as a point of intervention to control blood glucose levels in the NIDDM patient (*45*). Indeed, the overexpression of a bifunctional enzyme double-mutant (S32A.H258A), designed to exhibit a very large K/BP, in FAO cells via adenoviral transfection increased F-2,6-P_2 levels and concomitantly decreased gluconeogenic rates (*2*). Inhibition of the hepatic bisphosphatase reaction should produce the same result, thus lowering the blood glucose level. The benefit of this approach is apparent when one considers that the hyperglycemia, partially generated by overproduction of glucose in the liver, causes many of the chronic problems associated with diabetes (*46*−*51*).

ACKNOWLEDGMENT

We acknowledge the Microchemical Facility at the University of Minnesota for synthesis of oligonucleotides and DNA sequencing. NMR instrumentation was provided by the Structural Biology NMR Resource and the University of Minnesota, Medical School.

REFERENCES

1. Pilkis, S. J., Claus, T. H., Kurland, I. J., and Lange, A. J. (1995) *Annu. Rev. Biochem. 64*, 799−835.
2. Argaud, D., Lange, A. J., Becker, T. C., Okar, D. A., El-Maghrabi, M. R., Newgard, C. B., and Pilkis, S. J. (1995) *J. Biol. Chem. 270*, 24229−24236.
3. Pilkis, S. J., El-Maghrabi, M. R., and Claus, T. H. (1988) *Annu. Rev. Biochem. 57*, 755−783.
4. El-Maghrabi, M. R., Claus, T. H., Pilkis, J., Fox, E., and Pilkis, S. J. (1982) *J. Biol. Chem. 257*, 7603−7607.
5. Lively, M. O., El-Maghrabi, M. R., Pilkis, J., D'Angelo, G., Colosia, A. D., Ciavola, J. A., Fraser, B. A., and Pilkis, S. J. (1988) *J. Biol. Chem. 263*, 839−849.
6. El-Maghrabi, M. R., Fox, E., Pilkis, J., and Pilkis, S. J. (1982) *Biochem. Biophys. Res. Commun. 106*, 794−802.
7. Lin, K., Kurland, I. J., Li, L., Lee, Y. H., Okar, D., Marecek, J. F., and Pilkis, S. J. (1994) *J. Biol. Chem. 269*, 16953−16960.
8. Kurland, I. J., Li, L., Lange, A. J., Correia, J. J., El-Maghrabi, M. R., and Pilkis, S. J. (1993) *J. Biol. Chem. 268*, 14056−14064.
9. Kurland, I. J., and Pilkis, S. J. (1995) *Protein Sci. 4*, 1023−1037.
10. Li, L., Ling, S., Wu, C.-L., Yao, W.-Z., and Xu, G.-J. (1997) *Biochem. J. 328*, 751−756.
11. Nishimura, M., and Uyeda, K. (1995) *J. Biol. Chem. 270*, 26341−26346.
12. Tauler, A., Rosenberg, A. H., Colosia, A., Studier, F. W., and Pilkis, S. J. (1988) *Proc. Natl. Acad. Sci. U.S.A. 85*, 6642−6646.
13. Lee, Y. H., Okar, D., Lin, K., and Pilkis, S. J. (1994) *J. Biol. Chem. 269*, 11002−11010.
14. Pilkis, S. J., Walderhaug, M., Murray, K., Beth, A., Venkataramu, S. D., Pilkis, G. J., and El-Maghrabi, R. M. (1983) *J. Biol. Chem. 258*, 6135−6141.
15. Stewart, H. B., El-Maghrabi, M. R., and Pilkis, S. J. (1985) *J. Biol. Chem. 260*, 12935−12941.
16. Okar, D. A., Kakalis, L. T., Narula, S. S., Armitage, I. M., and Pilkis, S. J. (1995) *Biochem. J. 308*, 189−195.
17. Lin, K., Li, L., Correia, J. J., and Pilkis, S. J. (1992) *J. Biol. Chem. 267*, 6556−6562.
18. Lee, Y. H., Ogata, C., Pflugrath, J. W., Levitt, D. G., Sarma, R., Banaszak, L. J., and Pilkis, S. J. (1996) *Biochemistry 35*, 6010−6019.
19. Lee, Y. H., Olson, T. W., Ogata, C. M., Levitt, D. G., Banaszak, L. J., and Lange, A. J. (1997) *Nat. Struct. Biol. 4*, 615−618.
20. Hasemann, C. A., Istvan, E. S., Uyeda, K., and Deisenhofer, J. (1996) *Structure 4*, 1017−1029.
21. Hunkapiller, M. W., Smallcombe, S. H., Whitaker, D. R., and Richards, J. H. (1973) *Biochemistry 12*, 4732−4743.
22. Walters, E. D., and Allerhand, A. (1980) *J. Biol. Chem. 255*, 6200−6204.

23. Markley, J. L., and Westler, W. M. (1996) *Biochemistry 35*, 11092−11097.
24. Markley, J. L. (1978) *Biochemistry 17*, 4648−4656.
25. Sakata, J., Abe, Y., and Uyeda, K. (1991) *J. Biol. Chem. 266*, 15764−15770.
26. Okar, D. A., Felicia, N. D., Gui, L., and Lange, A. J. (1997) *Protein Expression Purif. 11*, 79−84.
27. Sarkar, G., and Sommer, S. S. (1990) *BioTechniques 8*, 404−407.
28. Bax, A., and Summers, M. (1986) *J. Am. Chem. Soc. 108*, 2093.
29. Wishart, D. S., Bigam, C. G., Yao, J., Abildgaard, F., and Dyson, H. J. (1995) *J. Biomol. NMR 6*, 135−140.
30. Cederholm, M. T., Stuckey, J. A., Doscher, M. S., and Lee, L. (1991) *Proc. Natl. Acad. Sci. U.S.A. 88*, 8116−8120.
31. Pelton, J. G., Torchia, D. A., Meadow, N. D., and Roseman, S. (1993) *Protein Sci. 2*, 543−558.
32. Gassner, M., Stehlik, D., Schrecker, O., Hengstenberg, W., Maurer, W., and Ruterjans, H. (1977) *Eur. J. Biochem. 75*, 287−296.
33. Sachs, D. H., Schechter, A. N., and Cohen, J. S. (1971) *J. Biol. Chem. 246*, 6576−6580.
34. Reynolds, W. F., Peat, I. R., Freedman, M. H., and Lyerla, J. R., Jr. (1973) *J. Am. Chem. Soc. 95*, 328−331.
35. Moore, C. D., Al-Misky, O. N., and Lecomte, J. T. J. (1991) *Biochemistry 30*, 8357−8365.
36. Zhang, P., Graminski, G. F., and Armstrong, R. N. (1991) *J. Biol. Chem. 266*, 19475−19479.
37. Cocco, M. J., Kao, Y.-H., Phillips, A. T., and Lecomte, J. T. J. (1992) *Biochemistry 31*, 6481−6491.
38. Zhou, M., Davis, J. P., and VanEtten, R. L. (1993) *Biochemistry 32*, 8479−8486.
39. Porubcan, M. A., Neves, D. E., Rausch, S. K., and Markley, J. L. (1978) *Biochemistry 17*, 4640−4647.
40. Rhyu, G. I., Ray, W. J. Jr., and Markley, J. L. (1985) *Biochemistry 24*, 4746−4753.
41. Markley, J. L., and Ibanez, I. B. (1978) *Biochemistry 17*, 4627−4639.
42. Kurland, I. J., Chapman, B., El-Maghrabi, M. R., and Pilkis, S. J. (1996) (manuscript in preparation).
43. Lee, Y. H. (1998) Unpublished results.
44. Li, L., Lin, K., Correia, J. J., and Pilkis, S. J. (1992) *J. Biol. Chem. 267*, 16669−16675.
45. Okar, D. A., Lee, Y. H., Argaud, D., McFarlan, S. C., and Lange, A. J. (1998) in *Frontiers in Diabetes* (Belfiore, F., Ed.) S. Karger AG, Basel.
46. Stolk, R., Vingerling, J. R., de Jong, P. T., Dielemans, I., Hofman, A., Lamberts, S. W., Pols, H. A., and Grobbee, D. E. (1995) *Diabetes 44*, 11−15.
47. Saito, N., Hattori, Y., Hiroi, Y., Takata, H., Hashimoto, K., Chikamori, K., Kuzuoka, T., Matsumo, S., Numata, S., Ikeda, Y., et al. (1995) *Nippon Ronen Igakkai Zasshi 32*, 747−755.
48. Molitch, M. (1997) *Semin. Nephrol. 17*.
49. Rodrigues, B., Cam, M. C., and McNeill, J. H. (1995) *J. Mol. Cell. Cardiol. 27*, 169−179.
50. Nathan, D. M. (1995) *Clin. Invest. Med. 18*, 332−339.
51. Nathan, D. M. (1996) *Ann. Intern. Med. 124*, 86−89.

BI9828728